



**Studies on the Densification and Grain Growth
Mechanisms of Polycrystalline Ceramic Based on
LaYO₃**

By

**NAJWA SHAFIQA BINTI ANWAR
(1330410933)**

A thesis submitted in fulfilment of the requirements for the degree of
Master of Science in Materials Engineering

**School of Materials Engineering
UNIVERSITI MALAYSIA PERLIS
2016**

APPROVAL AND DECLARATION SHEET

This thesis titled Studies on the Densification and Grain Growth Mechanisms of Polycrystalline Ceramic Based on LaYO_3 was prepared and submitted by Najwa Shafiqah Binti Anwar (Matric Number: 1330410933) and has been found satisfactory in terms of scope, quality and presentation as partial fulfillment of the requirement for the award of degree of Master of Science (Materials Engineering) in Universiti Malaysia Perlis (UniMAP).

Check and Approved by

.....
(DR. MOHD SOBRI BIN IDRIS)

Project Supervisor
School of Materials Engineering
Universiti Malaysia Perlis

(Date:)

School of Materials Engineering
Universiti Malaysia Perlis

2016

ACKNOWLEDGEMENTS

Alhamdulillah. Thanks to Allah. I would like to take this opportunity to express my heartiest gratitude to those who have provided me with help along the way, and the people who have shaped the person for who I am today.

First of all, I would like to express my best and sincere thanks to my supervisor, Dr. Mohd Sobri bin Idris for his continuous assistance, uncountable help and guidance, throughout the whole process to complete my research. He managed to teach me how to work independently, but at any time, his useful advice was continuously available to me. His enthusiasm has always invigorated me with a desire to investigate new and interesting topics. I deeply feel that my success is directly linked to his guidance.

I am also grateful to my ex-supervisor, Mrs. Salmie Suhana Che Abdullah for her guidance, constant encouragement and invaluable suggestions for my research work at first. Her confidence in my capabilities has given me immense opportunities to stimulate my research potential.

A lot of thanks to Prof. Dr. Shamsul Baharin Jamaludin and Dr. Rozana Aina Maulat Osman from Center for Frontier Materials Research, UniMAP, for their continuous assistance, uncountable help and guidance, throughout the whole process to complete my research. I am very grateful to them for keep having faith and confidence to entrust me with my research project. The knowledge and experience I've gained throughout this project were remarkable.

My gratitude is also extended to lecturers and technicians of School of Materials Engineering, UniMAP, for assisting in putting my research work into action and for their help and guidance during laboratory works. Many thanks also to my Electronic Materials group and my fellow friends, especially for their friendship and advice.

Also, to those who have helped directly or indirectly, I wish I could have put their names here, thanks for being helpful, cooperative and supportive.

Finally, I give my deepest love to my supportive and loving family members for their continuous support, encouragement, and understanding through these years. Their endless and unconditional love has encouraged and supported me ever since I was born.

TABLE OF CONTENTS

	PAGE
THESIS DECLARATION	i
ACKNOWLEDGEMENTS	iii
TABLE OF CONTENTS	iv
LIST OF TABLES	vii
LIST OF FIGURES	viii
LIST OF ABBREVIATIONS	xii
LIST OF SYMBOLS	xiii
LIST OF EQUATIONS	xiv
ABSTRAK	xv
ABSTRACT	xvi
CHAPTER 1 INTRODUCTION	1
1.1 Background	1
1.1.1 Solid Oxide Fuel Cells (SOFCs)	5
1.1.2 Basic Components of SOFCs	6
1.2 Problem Statement	8
1.3 Objectives	9
1.4 Scope of Study	9
CHAPTER 2 LITERATURE REVIEW	10
2.1 Introduction	10
2.2 Solid electrolyte used in SOFC	12
2.2.1 HT-SOFCs	13
2.2.2 IT-SOFC	15
2.3 Crystal structures of electrolyte materials	18
2.3.1 Fluorite-type oxides	18
2.3.2 Perovskite-type oxides	19
2.4 LaYO ₃ as solid electrolyte	22
2.5 Enhancement of solid electrolyte properties	24

2.5.1	Enhancement by modification of composition	25
2.5.2	Enhancement by modification of microstructure	26
2.5.3	Enhancement by modification of processing	27
2.6	Two-step sintering	29
CHAPTER 3 RESEARCH METHODOLOGY		39
3.1	Materials synthesis	39
3.2	Materials fabrication	40
3.3	Two-step sintering	40
3.4	Materials characterisation / instrumentation	42
3.4.1	X-ray diffraction, indexing and refinement	43
3.4.2	Density measurement	44
3.4.3	Shrinkage measurement	45
3.4.4	Scanning Electron Microscope (SEM)	46
3.4.5	Grain size measurement	47
3.4.6	Impedance Spectroscopy (IS)	47
CHAPTER 4 RESULTS AND DISCUSSION		53
4.1	Introduction	53
4.2	XRD analysis of LaYO ₃	54
4.3	Density measurement	59
4.4	Shrinkage measurement	62
4.5	Microstructural analysis	63
4.6	Grain size measurement	69
4.7	Impedance Analysis	72
4.7.1	Electrical resistance of the sintered LaYO ₃	72
4.7.2	Electrical conductivity of the sintered LaYO ₃	74
4.7.3	Arrhenius plots of the sintered LaYO ₃	75
4.7.4	Dielectric loss of the sintered LaYO ₃	77
4.7.5	Electrical capacitance of the sintered LaYO ₃	79
4.7.6	Permittivity, ϵ' of the sintered LaYO ₃	80
4.7.7	Z'', M'' plot of the sintered LaYO ₃	82
4.7.8	Comparison results of the electrical properties for sintered LaYO ₃ with different T ₂ temperature at different frequency	84
CHAPTER 5 CONCLUSIONS AND RECOMMENDATIONS		90
5.1	Conclusions	90
5.2	Recommendations for future work	91

5.3	Commercialisation potential	92
	REFERENCES	93
	APPENDIX A	101
	APPENDIX B	102
	LIST OF PUBLICATIONS	103

©This item is protected by original copyright

LIST OF TABLES

NO.		PAGE
1.1	Type of fuel cell and their characteristics and applications	4
1.2	Requirements for SOFC components	7
2.1	Values of ionic conductivity and activation energy of zirconia stabilized with different cations	16
2.2	Ionic conductivities of the means dopants of ceria at different temperatures	17
2.3	Sintered densities and grain sizes of alumina specimens under various heating parameters of two-step sintering	38
3.1	Typical electroceramics and their electrical properties	50
3.2	Capacitance values and their possible interpretation	52
4.3	The average grain size of powder compact LaYO_3 after two-step sintering.	69

LIST OF FIGURES

NO		PAGE
1.1	Operating principle of SOFC and its components	5
2.1	Conductivity data for YSZ, LSGM and CGO	14
2.2	The fluorite crystal structure	19
2.3	The ideal perovskite primitive cubic crystal structure	20
2.4	Comparison of conductivities of various oxygen-ion-conducting solid electrolytes	21
2.5	Phase diagram of the $\text{La}_2\text{O}_3\text{-Y}_2\text{O}_3$ system with the phase name abbreviations	23
2.6	The correlation of composition, microstructure, processing, and electrical conductivity in polycrystalline materials under given temperature and surrounding atmosphere	24
2.7	Density and grain size during heating ($10\text{ }^\circ\text{C}/\text{min}$) of undoped and doped Y_2O_3 . Initial powder size is 30 nm	31
2.8	Summary of two-step sintering experiment using Y_2O_3 (with 1% Mg^{2+}) starting with spherical powders of a particle size 200 nm. No grain growth (grain size 390 nm) was observed in the second step	32
2.9	Density and grain size of Y_2O_3 (with 1% Mg^{2+}) sintered in the second step at $1000\text{ }^\circ\text{C}$ for 60 h. Sample previously preheated to $1120\text{ }^\circ\text{C}$ (T_1) without holding	33
2.10	Scanning electron microscopy micrographs of dense BaTiO_3 ceramics prepared by two-step sintering. (A) 35 nm ($T_1 = 950\text{ }^\circ\text{C}$, $T_2 = 900\text{ }^\circ\text{C}/2\text{ h}$), (B) 70 nm ($T_1 = 980\text{ }^\circ\text{C}$, $T_2 = 900\text{ }^\circ\text{C}/4\text{ h}$), (C) 150 nm ($T_1 = 1100\text{ }^\circ\text{C}$, $T_2 = 900\text{ }^\circ\text{C}/20\text{ h}$), (D) 300 nm ($T_1 = 1180\text{ }^\circ\text{C}$, $T_2 = 950\text{ }^\circ\text{C}/20\text{ h}$), (E) 800 nm ($T_1 = 1230\text{ }^\circ\text{C}$, $T_2 = 1000\text{ }^\circ\text{C}/20\text{ h}$), and normal sintering (F) 1200 nm ($T = 1200\text{ }^\circ\text{C}/2\text{ h}$)	34
2.11	Grain size versus density for BaTiO_3 (30 nm powder) specimens sintered by normal sintering and two-step sintering	34

2.12	Grain size versus density for Ni-Cu-Zn ferrite (10 nm powder) specimens sintered by normal sintering and two-step sintering	36
2.13	Scanning electron microscopy micrographs of dense Ni-Cu-Zn ferrite made from 10 nm powders, by two-step sintering, (A) 200 nm ($T_1 = 850\text{ }^\circ\text{C}$, $T_2 = 800\text{ }^\circ\text{C}/6\text{ h}$), (B) 400 nm ($T_1 = 890\text{ }^\circ\text{C}$, $T_2 = 825\text{ }^\circ\text{C}/8\text{ h}$) (C) 500 nm ($T_1 = 910\text{ }^\circ\text{C}$, $T_2 = 850\text{ }^\circ\text{C}/4\text{ h}$), (D) 800 nm ($T_1 = 930\text{ }^\circ\text{C}$, $T_2 = 850\text{ }^\circ\text{C}/4\text{ h}$), and normal sintering (E) 2000 nm (900 $^\circ\text{C}/4\text{ h}$). Also shown is ferrite made from powders of solid state reactions, (F) 5000 nm (900 $^\circ\text{C}/4\text{ h}$)	36
2.14	Relative density for alumina specimens as function of sintering time at various temperatures for normal sintering	38
3.1	Sintering profile for conventional sintering for densification analysis.	41
3.2	Sintering profile for two-step sintering technique	41
3.3	Flow chart illustrating the various steps of synthesising, fabricating and characterising of LaYO_3 .	42
3.4	(a) impedance complex plane plot, Z^* ; (b) modulus complex plane plot, M^* ; (c) Combine Z'' , M'' spectroscopic plot	49
3.5	Possible equivalent circuit for a typical electroceramic and its frequency response in complex plane plots for the impedance and electric modulus formalisms	51
4.1	XRD pattern for LaYO_3 synthesized at 1500 $^\circ\text{C}$ for 10 hours and quenched in liquid nitrogen.	54
4.2	XRD pattern for LaYO_3 synthesised between 1200 – 1500 $^\circ\text{C}$ in air for 10 hours and slowly cooled by 10 $^\circ\text{C}/\text{min}$	55
4.3	XRD pattern for LaYO_3 synthesised between 1250 $^\circ\text{C}$ – 1500 $^\circ\text{C}$ in air for 10 hours and quenched in liquid nitrogen.	56
4.4	Variations of the lattice a as a function of temperature for LaYO_3 synthesised between 1250 – 1500 $^\circ\text{C}$	57
4.5	Variations of the lattice b as a function of temperature for LaYO_3 synthesised between 1250 – 1500 $^\circ\text{C}$	57
4.6	Variations of the lattice c as a function of temperature for LaYO_3 powders synthesised between 1250 – 1500 $^\circ\text{C}$	58

4.7	Variations of the unit cell volume, V as a function of temperature for LaYO_3 synthesised between 1250 – 1500 °C	58
4.8	Density of LaYO_3 as a function of dwell time for uniaxial pressing and cold isostatic pressing.	60
4.9	Relative density of sintered LaYO_3 with 15 hours dwell time as a function of sintering temperature.	60
4.10	Relative density of LaYO_3 with peak temperature (T_1) of 1300°C and 15 hours holding time as a function of dwell temperature (T_2).	61
4.11	The shrinkage percentage for fabricated LaYO_3 with peak temperature (T_1) of 1300°C and 15 hours holding time as a function of dwell temperature (T_2).	62
4.12	Scanning electron micrographs of LaYO_3 green pellet	64
4.13	Scanning electron micrographs of sintered LaYO_3 by conventional sintering at 1300 °C with 15 hours holding time	64
4.14	Scanning electron micrograph of LaYO_3 (left side) sintered at $T_1 = 1300$ °C/1 minute and reaching 75 % relative density. The binary images (right side) of the grain structures edited in ImageJ processing software with histogram of the average grain size calculated.	65
4.15	Scanning electron micrographs of sintered LaYO_3 by two-step sintering. The samples were sintered at $T_2 =$ (a) 1000 °C (b) 1050 °C (c) 1100 °C (d) 1150 °C (e) 1200 °C (f) 1250 °C for 15 hours, after reaching 75 % relative density in an initial firing at 1300 °C/1 min.	66
4.16	Scanning electron micrographs of sintered LaYO_3 by two-step sintering. The samples were sintered at $T_2 =$ (a) 1000 °C (b) 1050 °C (c) 1100 °C (d) 1150 °C (e) 1200 °C (f) 1250 °C for 15 hours, after reaching 75 % relative density in an initial firing at 1300 °C/1 min. The binary images (right side) of the grain structures edited in ImageJ processing software with histogram of the average grain size calculated.	67
4.17	Grain size of fabricated LaYO_3 with peak temperature (T_1) of 1300°C and 15 hours holding time as a function of dwell temperature (T_2).	69
4.18	Grain size vs. fractional density for LaYO_3 samples sintered by two-step sintering.	70

4.19	Grain size vs. relative density for LaYO ₃ samples sintered by two-step sintering	71
4.20	Variations of real (Z') and imaginary (Z'') parts of complex impedance of LaYO ₃ at different $T_2 =$ (a) 1000 °C (b) 1050 °C (c) 1100 °C (d) 1150 °C (e) 1200 °C (f) 1250 °C for 15 hours	73
4.21	Variations of conductivity of LaYO ₃ with frequency at different $T_2 =$ (a) 1000 °C (b) 1050 °C (c) 1100 °C (d) 1150 °C (e) 1200 °C (f) 1250 °C for 15 hours.	74
4.22	Arrhenius plots of DC conductivity of LaYO ₃ at different $T_2 =$ (a) 1000 °C (b) 1050 °C (c) 1100 °C (d) 1150 °C (e) 1200 °C (f) 1250 °C for 15 hours.	76
4.23	Variations of dielectric loss of LaYO ₃ with frequency at different $T_2 =$ (a) 1000 °C (b) 1050 °C (c) 1100 °C (d) 1150 °C (e) 1200 °C (f) 1250 °C for 15 hours.	78
4.24	Variations of capacitance of LaYO ₃ with frequency at different $T_2 =$ (a) 1000 °C (b) 1050 °C (c) 1100 °C (d) 1150 °C (e) 1200 °C (f) 1250 °C for 15 hours.	79
4.25	Permittivity (ϵ') plots of LaYO ₃ at different $T_2 =$ (a) 1000 °C (b) 1050 °C (c) 1100 °C (d) 1150 °C (e) 1200 °C (f) 1250 °C for 15 hours.	81
4.26	Variations of Z'' , M'' spectroscopic plot of LaYO ₃ with frequency at different $T_2 =$ (a) 1000 °C (b) 1050 °C (c) 1100 °C (d) 1150 °C (e) 1200 °C (f) 1250 °C for 15 hours.	82
4.27	Conductivity, Y' plots for sintered LaYO ₃ at frequency; (a) (i, ii) 0.1 Hz; (b) (i, ii) 1 Hz; (c) (i, ii) 10 Hz; (d) (i, ii) 100 Hz; (e) (i, ii) 1 kHz	85
4.28	Arrhenius plots for sintered LaYO ₃ at frequency; (a) 10 Hz; (b) 100 Hz; (c) 1 kHz	87
4.29	Dielectric loss plots for sintered LaYO ₃ at frequency; (a) 1 kHz; (b) 10 kHz; (c) 100 kHz; (d) 1 MHz	88
4.30	Permittivity (ϵ') plots for sintered LaYO ₃ at frequency; (a) 1 kHz; (b) 10 kHz; (c) 100 kHz; (d) 1 MHz	89

LIST OF ABBREVIATIONS

La	Lanthanum
Y	Yttrium
O ₂	Oxygen
H ₂	Hydrogen
La ₂ O ₃	Lanthanum Oxide
Y ₂ O ₃	Yttrium Oxide
LaYO ₃	Lanthanum Yttrium Oxide
SOFC	Solid Oxide Fuel Cell
ABO ₃	Perovskite structure
XRD	X-ray Diffraction
SEM	Scanning Electron Microscope
IS	Impedance Spectroscopy
Pt	Platinum
Ni	Nickel
Cu	Copper
Zn	Zinc
Ag	Silver
Mg	Magnesium
Nb	Niobium
CO	Carbon monoxide
CO ₂	Carbon dioxide
YSZ	Ytria Stabilized Zirconia
LSGM	Lanthanum Gallate, Strontium and Magnesium doped
SDC	Samarium Doped Ceria
ScSZ	Scandia Stabilized Zirconia
TSS	Two-step Sintering
RC	Resistance-capacitance

LIST OF SYMBOLS

2θ	Diffraction angle
λ	wavelength
%	percentage
$^{\circ}\text{C}$	degree Celsius
μ	micro
$\tan \delta$	dielectric loss
σ	conductivity
Z	impedance
Y	conductivity
ϵ	permittivity
M	Electric Modulus

©This item is protected by original copyright

LIST OF EQUATIONS

NO.		PAGE
1.1	$2\text{H}^+ + \frac{1}{2}\text{O}_2 + 2\text{e}^- \rightarrow \text{H}_2\text{O}$	3
1.2	$\text{H}_2 + \text{O}^{2-} \rightarrow \text{H}_2\text{O} + 2\text{e}^-$	3
1.3	$\text{H}_2 + \frac{1}{2}\text{O}_2 \rightarrow \text{H}_2\text{O}$	3
2.1	$j = \sigma^* E$	11
2.2	$\sigma = (A/T) \exp(-E_a/kT)$	11
3.1	$2d \sin \theta = n \lambda$	43
3.2	$\rho = \frac{ZM}{N_A V}$	44
3.3	$\rho = \frac{m}{v}$	45
3.4	Relative density = $\frac{\text{Experimental density}}{\text{Theoretical density}}$	45
3.5	Percentage of shrinkage (%) = $\frac{l_f - l_o}{l_o} \times 100\%$	45
3.6	$M^* = 1/\varepsilon^* = j\omega C_0 Z^* = j\omega C_0 (1/Y^*)$	48
4.1	$\sigma_b = \frac{1}{R_b} \times \frac{1}{A}$	75
4.2	$\varepsilon' = \frac{C}{\varepsilon_0} \times \frac{t}{A}$	80

KAJIAN MENGENAI PENUMPATAN DAN MEKANISMA TUMBESARAN IRA BAGI SERAMIK POLIHABLUR BERDASARKAN LaYO_3

ABSTRAK

LaYO_3 adalah seramik polihabluran dengan struktur jenis oksida perovskit. LaYO_3 disintesis menggunakan kaedah sintesis keadaan pepejal. Pada mulanya, sampel dipanaskan antara $1200\text{ }^\circ\text{C}$ hingga $1500\text{ }^\circ\text{C}$ selama 10 jam dan perlahan-lahan disejukkan dalam udara. Kehadiran fasa kedua iaitu otorombik menunjukkan sifat polimorfisme LaYO_3 . Fasa struktur monoklinik tulen telah berjaya disintesis selepas dipanaskan pada $1500\text{ }^\circ\text{C}$ selama 10 jam dan lindap-kejut dalam cecair nitrogen. Selepas itu, serbuk LaYO_3 monoklinik tulen telah dipelet menggunakan penekanan sestatik dan telah difabrikasi oleh kaedah pensinteran dua langkah. Bagi pensinteran langkah pertama (T_1), pelet telah dipanaskan pada $1300\text{ }^\circ\text{C}$ selama 1 minit dan kemudian dilindap-kejut ke dalam cecair nitrogen. Pelet kemudiannya dipanaskan pada suhu yang agak rendah antara $1000\text{ }^\circ\text{C}$ hingga $1250\text{ }^\circ\text{C}$ dan ditandakan sebagai T_2 selama 15 jam masa pegangan. Dengan meningkatkan T_2 , ketumpatan relatif meningkat daripada $\sim 87\%$ kepada $\sim 95\%$. Peratusan pengecutan juga meningkat secara linear. Mikrostruktur menunjukkan keseragaman. Saiz butiran adalah berkadar terus dengan ketumpatan relatif. Cole-cole plot daripada impedans menunjukkan satu separuh bulatan menyumbang kepada fenomena pukal sampel LaYO_3 yang telah disinter. Kekonduksian sampel yang disinter antara $1000\text{ }^\circ\text{C}$ hingga $1200\text{ }^\circ\text{C}$ berada dalam lingkungan 2 hingga $3 \times 10^{-5}\text{ S/cm}$ dan tenaga pengaktifan adalah kira-kira $\sim 0.4\text{ eV}$. Sementara itu, sampel yang disinter pada $1250\text{ }^\circ\text{C}$ menunjukkan kekonduksian yang tinggi iaitu $8.41 \times 10^{-3}\text{ S/cm}$ dengan 1.4 eV kerana mempunyai kesan sempadan ira di dalam sampel. Oleh itu, peningkatan suhu T_2 menunjukkan pengalir ionik yang tinggi dengan tingkah laku elektrik yang insulatif menyumbang kepada pembentukan pertumbuhan ira yang lebih besar.

STUDIES ON THE DENSIFICATION AND GRAIN GROWTH MECHANISMS OF POLYCRYSTALLINE CERAMIC BASED ON LaYO_3

ABSTRACT

LaYO_3 is a polycrystalline ceramic with the perovskite type oxide structure. LaYO_3 was prepared using solid state synthesis method. Initially, the sample was heated between $1200\text{ }^\circ\text{C}$ to $1500\text{ }^\circ\text{C}$ for 10 hours and slowly cooled in air. The existence of secondary phases that belongs to orthorhombic shows the polymorphism properties of LaYO_3 . Pure phase monoclinic structure was successfully synthesized after heated at $1500\text{ }^\circ\text{C}$ for 10 hours and rapidly cooled in liquid nitrogen. Then, the pure monoclinic LaYO_3 powder was pelletized using cold isostatic pressing and been fabricated by two-step sintering method. For the first-step sintering (T_1), pellets were heated at $1300\text{ }^\circ\text{C}$ for 1 minute and then quenched into liquid nitrogen. The pellets were then reheated at the relatively lower temperature between $1000\text{ }^\circ\text{C}$ to $1250\text{ }^\circ\text{C}$ and denoted as T_2 for 15 hours holding time. By increasing T_2 , the relative density increased from $\sim 87\%$ to $\sim 95\%$. Percentage of shrinkage also linearly increased within error. Microstructural analysis shows homogenous microstructure. The grain size was directly proportional to the relative density. Cole-cole plot from complex impedance of sintered LaYO_3 shows one semicircle contribute to the bulk phenomenon responsible. The conductivity for samples sintered between $1000\text{ }^\circ\text{C}$ to $1200\text{ }^\circ\text{C}$ were in the range of 2 to $3 \times 10^{-5}\text{ S/cm}$ and the activation energy is about $\sim 0.4\text{ eV}$. Meanwhile, sample sintered at $1250\text{ }^\circ\text{C}$ shows high conductivity that is $8.41 \times 10^{-3}\text{ S/cm}$ with 1.4 eV because phenomenon responsible in the sample have grain boundary effect. Therefore, increasing T_2 temperature shows high ionic conductor with electrically insulative behaviour that contribute by larger formation of grain growth.

CHAPTER 1

INTRODUCTION

1.1 Background

The ever-increasing energy demand triggered by the deficiency of fossil fuels has led us to seek alternative power sources. These fossil fuels were formed by natural processes of buried organisms, which are non-renewable resources, and it raises serious environmental concerns and economic effects (Abas *et al.*, 2015). Fuel cell is the most attractive alternative power source because it can produce clean and efficient electricity to meet the future challenges (Afif *et al.*, 2016; Kirubakaran *et al.*, 2009; Radenahmad *et al.*, 2016).

Fuel cells are considered an excellent alternative energy resource from the environmental point of view because fuel cells are quiet and produce negligible emissions of pollutants. Furthermore, the efficiency ranges from 40 to 60% depending on the type and design of fuel cells because different types of fuel cells have varied efficiencies. Moreover, the primary fuel source for the fuel cell is hydrogen that can be

obtained from natural gas, coal gas, methanol, and other fuels containing hydrocarbons (Stambouli & Traversa, 2002).

Initially, fuel cells were used in closed environments such as space technology and submarines, where cost is not an issue. NASA began using fuel cells in the late 1950s and continues to do so today. Fuel cells were used in the Apollo and Gemini spacecrafts, and now in space shuttles. Currently, there are many uses for fuel cells, including:

- I. Transportation: All the major automakers are working to commercialize a fuel-cell car. Fuel cells are powering buses, boats, trains, planes, and scooters, even bicycles.
- II. Stationary: More than 2500 fuel cell systems have been installed all over the world – in hospitals, nursing homes, hotels, office buildings, schools, utility power plants, and an airport terminal, providing primary power or backup.
- III. Residential: Fuel cells are ideal for power generation, either connected to the electric grid to provide supplemental power and backup assurance for critical areas, or installed as a grid-independent generator for on-site service in areas that are inaccessible by power lines. The waste heat from a fuel cell can be used to provide hot water or space heating for a home.
- IV. Portable Power: Miniature fuel cells for cellular phones, laptop computers and lightweight electronics are on their way to market. These small fuel cells generally run on methanol, an inexpensive wood alcohol also used in windshield wiper fluid.
- V. Landfill/Wastewater Treatment: Wastewater treatment plants and landfills are using fuel cells to convert the methane gas they produce into electricity. (Garche, 2013; Giddey *et al.*, 2012; Gong, 2005; Laosiripojana *et al.*, 2009; Liu *et al.*, 2016; Minh, 2004; Serincan, 2016).

Fuel cell is a device that converts chemical energy into electrical energy similar to battery but slightly differs in its electrochemical process. The output from a fuel cell is a stable direct current (DC) of about one-volt. Fuel such as natural gas (CH₄) or methanol (CH₃OH) and oxygen (from air) are required to operate fuel cell.

The fuel gas is fed into the fuel electrode (porous anode in a solid state) where the hydrogen is oxidized ($\text{H}_2 \rightarrow 2\text{H}^+ + 2\text{e}^-$). Oxygen in air is fed into the oxidant electrode (porous cathode in a solid form) where it is reduced ($\text{O}_2 + 2\text{e}^- \rightarrow \text{O}^{2-}$). Ions of hydrogen or oxygen are conducted by an electrolyte layer (liquid or dense solid) which is sandwiched between the two electrodes. From proton (hydrogen ion, H⁺) conducting electrolyte fuel cells, water is formed at the cathode/electrolyte side according to the equation;



For oxygen ion (O²⁻) conducting electrolyte fuel cells, water is formed at the anode/electrolyte side;



The overall reaction in the fuel cell is;



Fuel cells have five different types which are Alkaline Fuel Cell (AFC), Solid Polymer Fuel Cell (SPFC) and Phosphoric Acid Fuel Cell (PAFC) that are operated at relatively low temperatures (< 200 °C). Furthermore, Molten Carbonate Fuel Cell (MCFC) is performed at about 650 °C and Solid Oxide Fuel Cell (SOFC) operates between 650 and 1000 °C. Table 1.1 shows the main characteristics and applications of

each fuel cell, in terms of operating temperature. For a particular fuel cell, the application fields are based on its properties and performance. Based on this comparison, clearly the overall properties of SOFC can be superior to other types of fuel cell if their high operating temperature can be reduced (Stambouli & Traversa, 2002). To realize this possibility, the new electrolyte materials with higher ionic conduction than the conventional YSZ are required (Jacobson, 2010).

Table 1.1: Type of fuel cell and their characteristics and applications (Steele & Heinzel, 2001)

Type	T _{op} (°C)	Characteristics	Applications
AFC	50 ~ 100	<ul style="list-style-type: none"> • High power density (A/m²) • High Pt loadings • Pure O₂, no CO₂, no CO • Very expensive 	<ul style="list-style-type: none"> • Space vehicles • Automobile
SPFC	50 ~ 100	<ul style="list-style-type: none"> • Easy design • High Pt loading • Pure H₂ (>99.99%), no CO • Moderate current density 	<ul style="list-style-type: none"> • Space and military • Automobile
PAFC	~ 200	<ul style="list-style-type: none"> • Commercially successful • Available in a few to 300 kW • Tolerant to CO₂ but low CO • High reliability • High cost (\$2000 to \$3000 per kW) 	<ul style="list-style-type: none"> • Electricity-heat cogeneration • Power in remote areas (near natural gas supply lines) • Automobile
MCFC	600 ~ 700	<ul style="list-style-type: none"> • Corrosive • Internal natural gas-reforming • Need CO₂ for cathode • CO is usable fuel • No Pt but Ni catalyst • High-grade heat available 	<ul style="list-style-type: none"> • Medium to large (2 kW ~ 2 MW) cogeneration power systems • Load levellers in electric utilities • Not suitable for small power plants or for transportation use
SOFC	~ 1000	<ul style="list-style-type: none"> • Very high temperature • Simple in design • Internal natural gas-reforming • No catalyst needed • CO is usable fuel • Cell are difficult to produce • High-grade heat available 	<ul style="list-style-type: none"> • Cogeneration plant • Potential use in transportation sector if the operating temperature can be reduced

1.1.1 Solid Oxide Fuel Cell (SOFC)

Solid oxide fuel cell (SOFC) is an all-solid device that operated between 600 ~ 1000 °C. In contrast to other types of fuel cells, where the electrochemical reactions occur at the gas-liquid-solid three-phase-zone, reactions in SOFC occur at the gas-solid two-phase contact. The corrosive electrolyte is no longer a problem in SOFC, as two porous ceramic electrodes are separated by a dense oxide-ion conducting ceramic electrolyte. Fuel (H_2 or CO) is fed to the anode and reacts with oxygen ions to form water (or CO_2) while releasing electrons to the external circuits. On the other hand, oxygen is fed to the cathode and accepts electrons from the external circuit to form oxygen ions. Electrons flow from the anode through the external circuit to the cathode (Badwal *et al.*, 2014; Mahato *et al.*, 2015; Timurkutluk *et al.*, 2016).

Figure 1.1 shows the operating principles of SOFC with flow directions for each species and with captions for each cell component. The focus of this research study is on electrolyte materials and hence only oxygen-ion conducting SOFC will be reviewed in the next chapter.

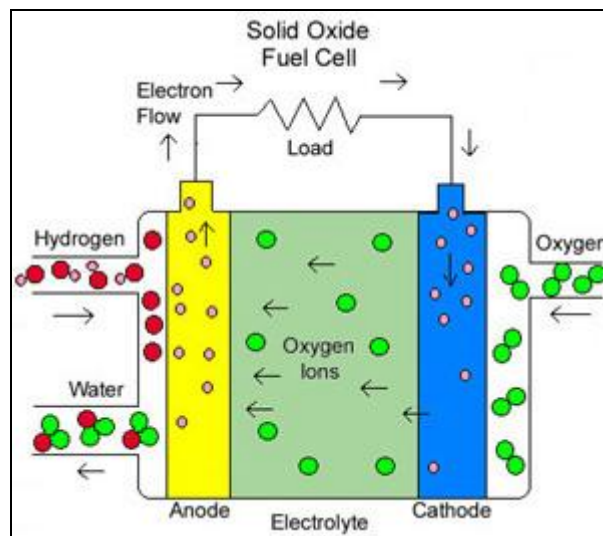


Figure 1.1: Operating principle of SOFC and its components (Kawamoto, 2008).

1.1.2 Basic components of SOFCs

There are specific material requirements and criteria that need to be satisfied before they can be considered as cathode, anode or electrolyte for SOFC application. These requirements are necessary to ensure the electrochemical reactions that occur at high temperatures will be at the most optimum condition, efficient and safe. These are criteria for cathode, anode and electrolyte (Badwal *et al.*, 2014; Stambouli & Traversa, 2002; Yokokawa *et al.*, 2001; Yamamoto, 2000)

i. Cathode

The criteria for the cathode material are:

- (1) High electrocatalytic activity for oxygen reduction
- (2) High electronic conductivity
- (3) Stability in the oxidizing atmosphere and at high-temperature
- (4) Thermal expansion compatible with other cell components
- (5) Porous for efficient oxygen transport

ii. Anode

For the anode material, the criteria are:

- (1) Effective oxidation catalysis
- (2) High electronic conductivity
- (3) Stability in the reducing anodic environment and at high-temperature
- (4) Thermal expansion compatible with other cell components
- (5) Porous for easy fuel transport
- (6) Tolerance to sulphur contaminants and hydrocarbon fuels

iii. Electrolyte

Criteria for electrolyte materials are:

- (1) High oxygen ion conductivity and negligible electronic conductivity
- (2) High stability under both oxidizing and reducing atmospheres
- (3) Stability at high-temperature
- (4) Thermal expansion compatibility with electrode materials
- (5) High density to prevent fuel transport to the cathode

Table 2.1 summarizes the most important material requirements for each component of SOFC in terms of electrical conductivity, stability, compatibility, and porosity (Minh & Takahashi, 1995).

Table 2.1: Requirements for SOFC components (Minh & Takahashi, 1995)

Component	Requirements				
	Conductivity	Stability	Compatibility	Porosity	Thermal expansion
Anode	High electrical conductivity	Chemical, phase, morphological, and dimensional stability in fuel environment	No undesirable chemical interactions or interdiffusion with adjoining cell components	Porous	Thermal expansion match with adjoining components
Electrolyte	High ionic conductivity. Negligible electrical conductivity	Chemical, phase, morphological, and dimensional stability in fuel and oxidant environment	No damaging chemical interactions or interdiffusion with adjoining cell components	Fully dense	Thermal expansion match with adjoining components
Cathode	High electrical conductivity	Chemical, phase, morphological, and dimensional stability in oxidant environment	No damaging chemical interactions or interdiffusion with adjoining cell components	Porous	Thermal expansion match with adjoining components
Interconnect	High ionic conductivity. Negligible electrical conductivity	Chemical, phase, morphological, and dimensional stability in fuel and oxidant environment	No damaging chemical interactions or interdiffusion with adjoining cell components	Fully dense	Thermal expansion match with adjoining components

1.2 Problem Statement

Nowadays, fuel cell is attracting much interest as power generation system with high energy conversion efficiency and almost no emission of air pollutant. Among the various types of fuel cell, SOFCs have many advantages such as variety of fuel, long life and environmental friendly system. Therefore, the development of SOFC is highly important. The conventional SOFCs are operated at high temperature about ~ 1000 °C and special alloy required for encapsulation. The drawbacks using high temperature are high operation cost, costly maintenance, phase stability of the materials and its compatibility was affected. So, the development of SOFCs at relatively lower operating temperature (< 1000 °C) require suitable electrolytes materials with reasonable high conductivity as an alternative for YSZ.

Conventional solid electrolyte, yttria stabilized zirconia (YSZ) have very low conductivity about 4.52×10^{-6} S/cm and it formed resistive layers between electrodes. Strontium magnesium doped lanthanum gallate (LSGM) was used as typical electrolyte has high ionic conductivity 1.7×10^{-1} S/cm but the limitation of LSGM is to get phase pure because existence of secondary phases. LaYO_3 has been proposed as a potential electrolyte because it shows ion conduction with oxide ion transport number is unity with conductivity is 5.8×10^{-4} S/cm at 1000 °C and activation energy are 1.22 eV (calculated) and 1.3 eV (experimental). Therefore, further improvements are required to enable LaYO_3 to become suitable electrolyte at < 1000 °C operation temperature.